Journal of Power Sources 238 (2013) 197–202

Contents lists available at SciVerse ScienceDirect

Journal of Power Sources

journal homepage: www.elsevier.com/locate/jpowsour

Preparation and electrochemical lithium storage features of TiO_2 hollow spheres

Liang Xiao*, Minglei Cao, Daidi Mei, Yonglin Guo, Lifeng Yao, Deyu Qu, Bohua Deng

Department of Chemistry, School of Science, Wuhan University of Technology, Wuhan 430070, Hubei, PR China

HIGHLIGHTS

- Uniform and monodispersed TiO_2 hollow spheres were prepared.
- Additional surface capacities of TiO_2 hollow spheres were observed.
- Kinetic of the additional surface capacity is fast.

ARTICLE INFO

Article history:
Received 22 September 2012
Received in revised form
8 March 2013
Accepted 11 March 2013
Available online 25 March 2013

Keywords:
Lithium-ion battery
Titanium dioxide
Hollow sphere
Surface lithium storage

ABSTRACT

Uniform and monodispersed TiO_2 hollow spheres with nanoporous titania shell are prepared successfully by using carboxyl-functionalized polystyrene spheres as templates. The results show that TiO_2 hollow spheres pose a stable reversible capacity of 230 $mAhg^{-1}$ at 33.5 mAg^{-1} and 120 $mAhg^{-1}$ at 1675 mAg^{-1}, which are higher than that of bulk TiO_2 with coarse grain. The discharge process of TiO_2 hollow spheres are suggested containing three consecutive stages: the formation of tetragonal Li_xTiO_2 solid solution, coexistence of two-phase mixture of $Li_{0.05}TiO_2$ and $Li_{0.5}TiO_2$ at 1.75 V and additional lithium storage in the surface. The superior high rate and high capacity performance of prepared TiO_2 hollow spheres are due to its highly reversible additional surface capacities and accommodation of phase transformation within nanostructure.

1. Introduction

Lithium ion batteries (LIBs) are more and more considered as promising power sources for electric vehicles (EVs) and energy storage systems for wind and solar power energy plants [1]. However, the cost, safety, energy density and power density at current level limit its further commercialization in large scale. Hence, a lot of works were dedicated to development alternative cathode and anode materials with enhanced electrochemical performance. Furthermore, to construct and use nanostructured electrode materials is a popular and effective stratagem to improve the performance of LIBs.

For instance, titanium dioxide (TiO_2) as an alternative electrode materials of LIBs has triggered extensive interests due to its low cost, environmental benignity and easy availability [2–4]. The stability and safety of TiO_2 are excellent due to the low volume change which is less than 4% [5,6] and safe electrode potential (1.5–1.8 V vs. Li^+/Li). However, applications of TiO_2 as electrode materials in LIBs have been hampered by its low ionic [7] and electrical conductivity [8]. Additionally, TiO_2 offers a specific capacity of 168 $mAhg^{-1}$ (0.5Li per TiO_2) practically, which limits its energy/power density further [9,10]. It has been demonstrated that to construct and use nanostructured TiO_2 is an effective way to improve the Li-ion diffusion rate and electrical conductivity of titanium oxide [4,11]. It is obvious that as the size of particles moving into the nano scale, the diffusion length of Li-ion will effectively reduce. A theoretical modeling study showed a dramatically increased Li-ion conductivity was observed in TiO_2 with particle size smaller than 20 nm [12]. Moreover, because of its large surface area and specific surface properties, additional surface lithium storage capacities of nanosized TiO_2 were observed [13–15].

However, in practical situation, aggregation of nanoparticles during charge/discharge cycling poses another new difficulty on the using of loosely packed TiO_2 nanoparticles as LIBs anode [4]. A better way to avoid this is to prepare nanoporous TiO_2, especially hollow spherical TiO_2. Micron-sized spherical hollow particles are easier to disperse in composite practical electrode than nanosized particles to ensure good contact between active material and

* Corresponding author. Tel.: +86 27 87756662.
E-mail address: leonshaw@yeah.net (L. Xiao).

0378-7753/$ – see front matter © 2013 Elsevier B.V. All rights reserved.
http://dx.doi.org/10.1016/j.jpowsour.2013.03.081

conductive agent. The hollow structure carries the advantages of nanoparticles such as shorten diffusion length and additional robust of the meso structures. Several studies have been carried on to produce hollow spherical TiO_2 [16–22]. Lou's group reported an over 100 $mAhg^{-1}$ reversible capacity at 10 C after constructing a TiO_2 hollow sphere where TiO_2 nanosheets with large amount of exposed 001 facets [21]. They attributed the superior rate behavior of prepared TiO_2 hollow spheres to the more efficient diffusion along the *c* axis than in the ab plane [21]. Besides this special nano construction, superior performance of mesoporous hollow TiO_2 microspheres was reported by Zhang et al. A very stable reversible capacity of 184 $mAhg^{-1}$ at 0.25 C and extremely high power of 122 $mAhg^{-1}$ at the high rate of 10 C were given by the hollow structures [22]. Zhang et al. suggested that the hollow structure and large mesoporous channels of the material facilitate electrolyte transportation and lithium ion diffusion and the small mesopores and small sized nanoparticles increase the lithium storage capacity. However, the lithium insertion and extraction mechanism and special features of charge/discharge curves were not discussed in detail. Moreover, relatively fast capacity fading is commonly observed in some other TiO_2 hollow spheres [16–20]. Therefore, the preparation and lithium storage features and mechanism of hollow spherical TiO_2 as electrode materials of LIBs are still worth to study further.

In this work, TiO_2 hollow microspheres were prepared by using carboxyl-functionalized polystyrene spheres as template. The electrochemical performances and characteristics of as-prepared sample were studied and bulk TiO_2 was also investigated as an experimental comparison. The possible reason for the advantage and electrochemical features of TiO_2 hollow structure as lithium storage material were discussed.

2. Experimental

All chemicals were A.R. and purchased from Sinopharm Chemical Reagent Co., Ltd. The TiO_2 hollow spheres were synthesized by using carboxyl-functionalized polystyrene spheres as templates. Monodispersed carboxyl-functionalized polystyrene spheres (PSA) were synthesized by dispersion copolymerization of Styrene (St) and Methyl acrylic acid (MA). Typically, 2 g PSA spheres were washed 2–3 times with diluted ammonia, washed 1 time with ethanol by centrifugation, and then dispersed into 100 mL of absolute ethanol dissolved 0.5 g of polyvinylpyrrolidone (PVP). Then 2.5 mL of tetrabutyl orthotitanate (TBOT) was added under vigorous stirring. After 30 min, a solution of 1 mL water in 20 mL ethanol was added dropwise to get a thicker coating. The synthesized PSA/TiO_2 spheres were repeatedly washed with ethanol by centrifugation and then dried. Finally, the hollow TiO_2 hollow spheres (designated as TiO_2-HS) were obtained by calcination in air heated to 550 °C for 5 h with a heating rate of 1 °C min^{-1} to remove the polymer cores. Commercial TiO_2 (designated as TiO_2-bulk) powders, which purchased from Shanghai Experimental Reagent Co., were used as a reference material.

The morphologies of TiO_2-HS were examined with scanning electron microscope (SEM, JSM-5610LV) and high resolution transmission electron microscope (HRTEM, JEM -2100F). The powder XRD patterns of TiO_2-bulk and TiO_2-HS were obtained on Rigaku D/MAX-III at 40 kV and 30 mA (Cu Kα radiation). N_2 adsorption–desorption isotherms were carried out on Micromeritics Tristar 3000 analyzer at 77 K under a continuous adsorption condition. BET and BJH analyses were used to determine the surface area and pore size distribution. The electrochemical performances of above samples were measured in a CR-2032-type coin cell. The TiO_2 electrodes were prepared by mixing 85 wt.% of active materials with 10 wt.% of acetylene black and 5 wt.% polyvinylidene difluoride (PVdF) in a N-methyl pyrrolidone (NMP) solution. The slurry was coated on stainless steel foil (geometrical area of the electrode is 1.5 cm^2) and vacuum dried at 130 °C for 12 h. The TiO_2 electrodes was then weighted and incorporated into coin cell in an argon filled glove box with a lithium foil as both reference and counter electrodes, a polymer separator and 1 M $LiClO_4$-EC/DMC (1:2 in volume, Merck) as electrolyte. All the electrochemical studies were carried out on NEWARE BTS battery tester at room temperature and all potentials refer to Li^+/Li.

3. Results and discussion

The SEM micrograph of prepared TiO_2 hollow spheres is shown in Fig. 1. Most of the hollow particles remain spherical and monodispersed after templates removing. Some broken spheres of the TiO_2 indicate the hollow structure. The TEM micrograph (Fig. 2A) confirmed the hollow structure of TiO_2 clearly. The average diameter of polymer templates (PSA) used in this study is about 1.3 μm. From TEM micrographs in Fig. 2, we found the TiO_2 hollow spheres are uniform and the average size is approximately 1.5 μm, the thickness of the titania shell is about 135 nm. It means the morphology and size of the templates were replicated successfully by the TiO_2 hollow spheres. The TEM micrograph with high magnification (Fig. 2B) shows the crystallized TiO_2 shell after calcinations at 550 °C, which is consistent with the following results of the X-ray diffraction.

Fig. 3 shows the XRD patterns of bulk TiO_2 and TiO_2 hollow spheres. All of the identified peaks of bulk TiO_2 expect the one located at $2\theta = 27.4°$ can be indexed to anatase TiO_2 (JCPDS card no. 21-1272). The small diffraction peak located at 27.4° marked with asterisk is attributed to small amounts of rutile phase. XRD patterns of TiO_2 hollow spheres show a pure anatase phase. The weaker and wider diffraction peaks of TiO_2 hollow spheres compared to bulk TiO_2 suggest that the hollow spheres are constructed with nanosized TiO_2 particles. The mesoporous structure with nanosized TiO_2 particles as building blocks was confirmed by the results of the N_2 adsorption–desorption experiments. Fig. 4 shows the N_2 adsorption–desorption isotherm and pore size distributions of the TiO_2 hollow spheres. The average pore diameter of TiO_2 hollow spheres is 6.1 nm, the pore size distributions centered at 4.5 nm. All the results of SEM, TEM and N_2 adsorption–desorption indicate uniform and monodispersed TiO_2 hollow spheres with nanoporous titania shell were prepared successfully.

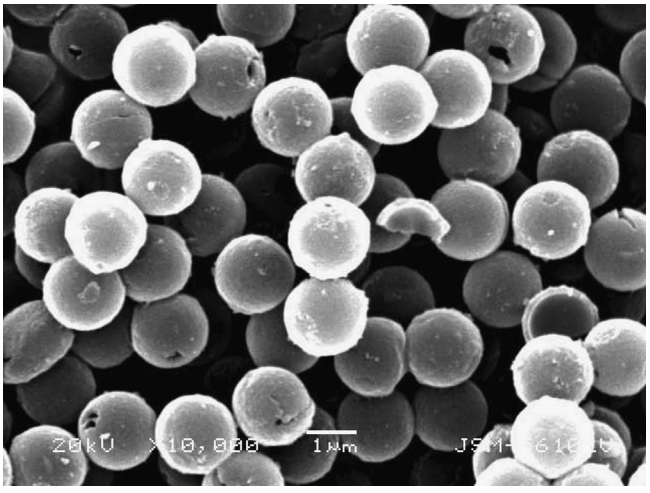

Fig. 1. SEM micrograph of prepared TiO_2 hollow spheres.

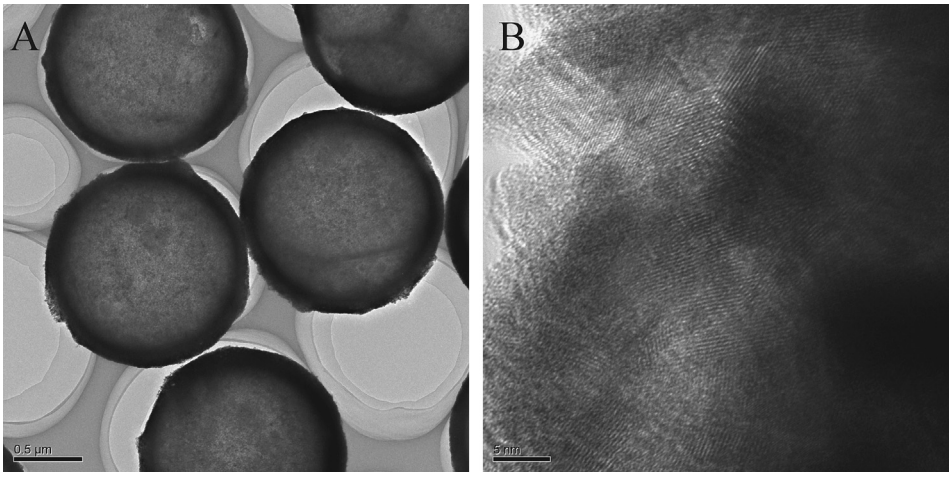

Fig. 2. TEM micrographs of prepared TiO_2 hollow spheres.

Fig. 5 shows the first (Fig. 5A) and second (Fig. 5B) charge/discharge profiles of bulk TiO_2 and TiO_2 hollow spheres with current density of 35.5 mAg^{-1} (0.1 C) in a voltage range of 1.0–3.0 V. The first and second charge/discharge specific capacities, coulombic efficiency and reversible capacities expressed as lithium insertion coefficient x (Li_xTiO_2) are summarized in Table 1. The coulombic efficiency of TiO_2-HS is smaller than that of TiO_2-bulk in the first cycle. Jiang et al. suggested that the first-cycle discharge capacity of hollow TiO_2 is partly contributed by the irreversible decomposition of electrolyte accompanying the formation of the solid-electrolyte interface (SEI) [15]. There is little possible of lithium-consuming solid electrolyte interface formation in a voltage range of 1.0–3.0 V. Wang et al. ascribe the irreversible capacity of hollow TiO_2 to the trapping of Li^+ in the surface vacancies or voids [20]. Higher surface area might cause more formation of SEI or more trapping Li^+ in the surface. Herein, the relatively lower coulombic efficiency of TiO_2-HS in the first cycle might be attributed to its higher surface area compared to that of TiO_2-bulk. The mechanism of capacity loss of TiO_2-HS in the first cycle is still an opening question which is worth to be studied further.

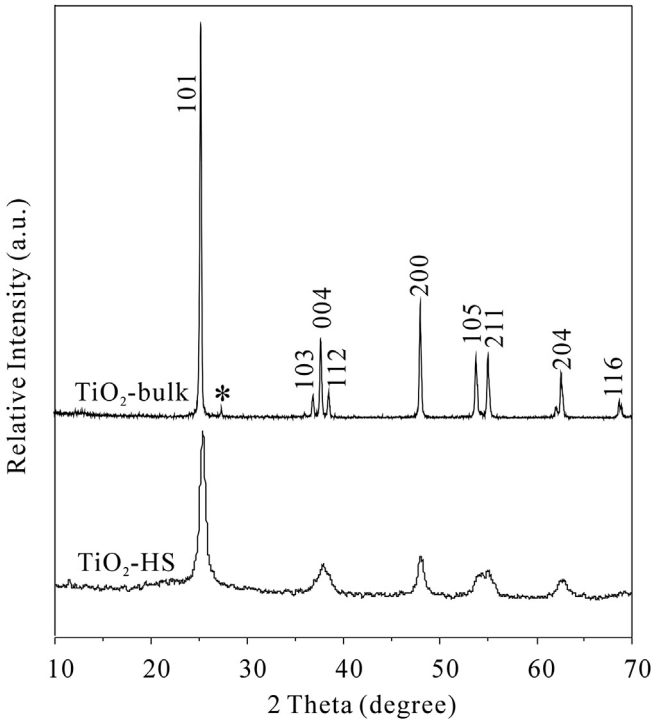

Fig. 3. XRD patterns of prepared TiO_2 hollow spheres and bulk TiO_2.

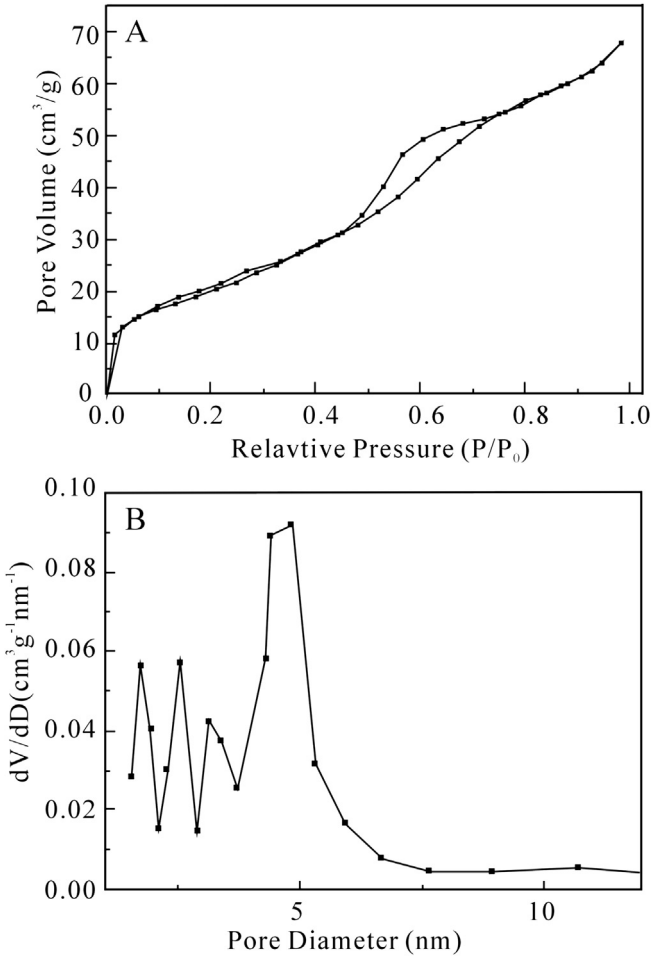

Fig. 4. N_2 adsorption–desorption isotherm (A) and pore size distributions (B) of prepared TiO_2 hollow spheres.

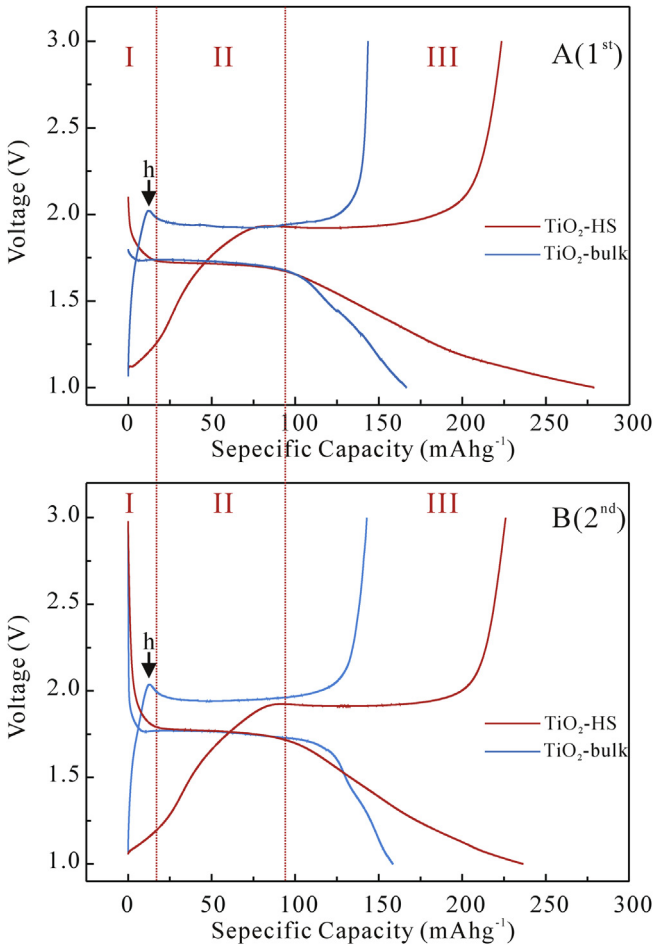

Fig. 5. The first (A) and second (B) charge/discharge curves of TiO_2 hollow spheres and bulk TiO_2 at 0.1 C in the voltage range of 1.0–3.0 V.

The lithium insertion coefficient x of TiO_2-bulk is less than 0.5, which is in agreement with the electrochemical performance of bulk anatase TiO_2 reported in literatures [9,10]. When $x = 0.5$ ($Li_{0.5}TiO_2$), the symmetry of the anatase unit cell decreases from its original $I4_1/amd$ symmetry to the orthorhombic Imma space group [23]. The change in symmetry results a net increase of ~4% of the unit cell volume and a rapid capacity fade [24]. $x = 0.5$ is the consistently reported maximum electrochemical insertion of Li because a strong repulsive force between Li ions will generate when the insertion ratio is greater than 0.5 [9]. It is noted that the TiO_2-HS could accommodate 0.79 Li/TiO_2 (279.2 $mAhg^{-1}$) during the first discharge with a reversible capacity of 0.63 Li/TiO_2 (223.8 $mAhg^{-1}$) at 0.1 C. The TiO_2-HS demonstrated capacities with stoichiometry ratio up to 0.63 (more than 0.5) Li/TiO_2 can be addressed from the advantages of its nanostructure. The capacity improvement of TiO_2 from hollow spheres should be studied much deeper.

As shown in the Fig. 5, the discharge curves related to process of Li insertion into TiO_2-HS electrodes can be divided into three regions. In region I, a monotonous potential decrease corresponding to 0.05 Li inserted into per TiO_2 is observed before reach a voltage plateau at about 1.75 V. Tarascon and coworkers [24] assigned this region to the formation of solid solution domain of anatase TiO_2 and Li_xTiO_2 with ex situ XRD results. In Tarascon's work, extension of the solid solution domain for nanosized TiO_2 particles was observed with the insertion reaction up to 0.15 Li/TiO_2. Jiang et al. [15] also found a very large capacity within this potential range in the first discharge (0.22 Li/TiO_2) of TiO_2 with particle size of 6 nm, but it decreased rapidly from the second cycle and then kept constant thereafter. Jiang et al. addressed this stable small capacity from the second cycle to the electrochemical double layer capacity rather than the formation of solid solution domain, since it is proportional to the specific surface areas of different electrodes and highly reversible. In present study, the capacities in region I are almost the same for the first and second discharge with different potential variations. For the first discharge, the electrode potential decreases from an initial potential of 2.1 V to 1.75 V for a fresh cell, whereas the electrode potential decreases from 3.0 V to 1.75 V for the second discharge. Electrochemical double layer effects will lead to different capacities for the different potential variations, but it is not the case for discharges of TiO_2-HS. The formation of solid solution domain, rather than a capacitive-like surface effect, might be more plausible to explain the discharge capacities before voltage plateaus at 1.75 V. Furthermore, the solid solution domain up to 0.05 Li/TiO_2 of TiO_2-HS is in agreement with the limit of lithium insertion amount to maintain the structure of tetragonal Li_xTiO_2 with space group $I4_1/amd$ [23]. Similar regions in discharge curves (blue line) of TiO_2-bulk are also observed before the voltage plateaus at 1.75 V. The capacities of TiO_2-bulk in these regions are distinctively smaller than the capacities of TiO_2-HS. It is obvious that as the size of particles moving into the nano scale, relatively faster kinetics and higher capacities could be expected because of the reduced diffusion length of Li-ion.

In the region II, well defined potential plateaus at about 1.75 V are observed for both TiO_2-HS and TiO_2-bulk. These are related to the coexistence of two-phase mixture of the tetragonal $Li_{0.05}TiO_2$ and the Li-rich orthorhombic $Li_{0.5}TiO_2$ [23,24]. Moreover, the voltage plateaus in the discharge curves of TiO_2-bulk and TiO_2-HS have almost the same length, i.e. the same plateau capacities (Q_p). Most puzzling aspect of this observation is where the higher capacity of TiO_2-HS than that of TiO_2-bulk comes from. The sloped regions (region III) in the specific capacity–voltage curves (Fig. 5) of TiO_2-HS should be the clues. It is found that the additional capacities are coming from the slope regions below 1.75 V after the voltage plateaus. Monotonic declining or increasing voltage–capacity curves without flats is observed in literatures for TiO_2 during cycles [13–15,25]. The slope regions below 1.75 V in the specific capacity–voltage curves of prepared TiO_2-HS might have a different lithium storage mechanism compared with lithium-ion insertion into bulk TiO_2.

There are several explanations for these observations in literatures. Wang et al. [13] suggested that the fast charge/discharge rate

Table 1
Specific capacities, coulombic efficiency and reversible capacities expressed as lithium insertion coefficient x (Li_xTiO_2) in the first and second charge/discharge of TiO_2-bulk and TiO_2-HS.

Samples	Specific capacity ($mAhg^{-1}$)		Coulombic efficiency	x in Li_xTiO_2	Specific capacity ($mAhg^{-1}$)		Coulombic efficiency	x in Li_xTiO_2
	1st discharge	1st charge			2nd discharge	2nd charge		
TiO_2-bulk	167.0	143.5	85.9%	0.40	158.8	143.0	90.1%	0.40
TiO_2-HS	279.2	223.8	80.2%	0.63	236.3	226.2	95.7%	0.64

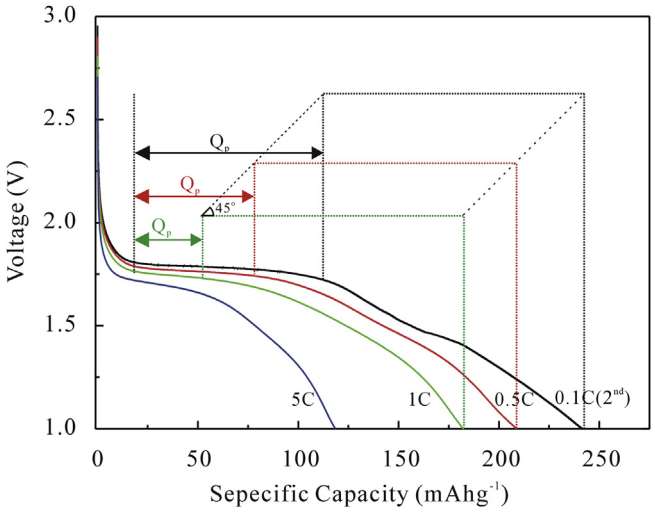

Fig. 6. The discharge curves of TiO_2-HS at different rates.

is expected from both double layer formation and pseudo capacitive reaction occurring at the surface of TiO_2. Jiang et al. [15] indicated that, after all the available interstitial octahedral sites inside the anatase crystals are filled, Li ions are further inserted into the surface layer under the external force of the electric field (from 1.78 to 1.0 V). Because decreasing the crystallite size can broaden the energy levels accessible in the materials, a wide voltage distribution at which the electrochemical reaction take place appears [26]. Okumura et al. [14] attribute the additional capacity and enhanced rate performance of TiO_2-B nanowires to its different surface structure compared with bulk TiO_2-B, which were confirmed by X-ray absorption spectroscopy studies. The specific structure of space charge layer (SCL) in the TiO_2-B surface makes lithium-ion insertion smooth. In this study, the discussions mainly focus on special electrochemical lithium storage features of TiO_2 hollow spheres. The mechanism of the formation of region III is not illustrated thoroughly, and it should be studied further. Anyhow, it can be concluded that region III below 1.75 V is related to the high surface area and special surface structure of nanoporous TiO_2-HS. Smaller capacities of TiO_2-bulk in region III are reasonable due to its coarse grained feature with smaller surface area.

In summary, the discharge process of TiO_2-HS is composed of three consecutive stages. They are the formation of tetragonal Li_xTiO_2 solid solution with space group $I4_1/amd$ before 1.75 V, coexistence of two-phase mixture of the tetragonal $Li_{0.05}TiO_2$ and the Li-rich orthorhombic $Li_{0.5}TiO_2$ at voltage plateau of 1.75 V and additional surface capacity from 1.75 to 1.0 V.

To study the reversibility of above mentioned three consecutive stages, the charge process was carefully investigated. In the charge curves of the TiO_2-HS electrode shown in Fig. 5, the sloped region between 1.0 and 1.9 V before a voltage plateau at 1.9 V is the reverse Li extraction from the surface layer. The following voltage plateau at 1.9 V is due to the coexistence of two-phase mixture appeared again. During the charge process of TiO_2-bulk, a characteristic "hump" marked as "h" is clearly observed. The existence of the hump indicates a transient overpotential related to nucleation-growth mechanism of phase transition, which usually seen in other Li-insertion materials. However, the hump in the charge curve of TiO_2-HS is more flat and difficult to see. In literatures, both X ray diffraction (XRD) and Neutron diffraction (ND) have demonstrated the absence of a two-phase equilibrium within nanosized crystallites smaller than a critical size [27,28]. The absence of distinct hump in the charge curve of TiO_2-HS is related to the accommodation of phase transformation within nanostructure. More evidence is that humps were reappeared for TiO_2 nanotubes with appropriate anneal for crystallization to destroy nanostructure in Xiong's work [25]. Finally, the capacities corresponding to discharge curves above 1.9 V are the reverse process of the formation of Li_xTiO_2 ($x < 0.05$) solid solution.

From the view of thermodynamic, reactions of above mentioned three consecutive stages have different mechanisms. They are essentially different reactions. For the smaller specific surface area, the additional surface capacity of TiO_2-bulk is smaller than that of TiO_2-HS. Therefore, the reversible of TiO_2-HS will be higher than that of TiO_2-bulk at a same rate, whether the charge/discharge rate is high or low. However, in the aspect of kinetic study, different kinetic features should be expected with the different lithium storage mechanisms along with three consecutive stages. Fig. 6 shows the discharge curves of TiO_2-HS with different rates (0.1 C, 0.5 C, 1 C and 5 C) after the first cycle of assembled fresh cell. The discharge curve of 0.1 C rate in Fig. 6 is the second discharge and marked as 0.1 C (2nd). It is clearly observed that the capacities corresponding to voltage plateau (Q_p) decrease with the increasing of current densities. Interestingly, the decreased values of Q_p are approximately equal to the decreased values of total lithium storage capacity for 0.1 C, 0.5 C and 1 C rate. These relationships were expressed by the dash line shown in Fig. 6. The faster kinetic of the additional surface capacity than that of insertion capacity might be possible reason for these observations. Additional insertion of Li-ion into the surface of TiO_2 is faster than the insertion of Li-ion into bulk phase because of the facility of lithium storage in surface and the sluggish of lithium ion diffusion in TiO_2 lattice. Therefore, the capacity loss at 0.5 C and 1 C mainly come from the polarization of insertion of lithium into TiO_2 lattice, the polarization of additional surface capacity of lithium storage is relatively small and can be ignored. However, at 5 C rate discharge capacities of lithium insertion into both bulk lattice and surface are dramatically decreased. This means that the polarization of additional surface capacity of TiO_2-HS can not to be ignored at relatively high rate.

The different electrochemical kinetics is also shown in the capacity retention profiles at different rates (Fig. 7). TiO_2-HS are able to deliver a stable specific discharge capacity of 220, 170 and 120 $mAhg^{-1}$ at rates of 0.5 C, 1 C and 5 C respectively. In Fig. 7, the ΔQ is the difference of discharge specific capacities for TiO_2-bulk and TiO_2-HS at same discharge rate. It is observed that the values of ΔQ at 0.5 C and 1 C are nearly the same, which was expressed by a

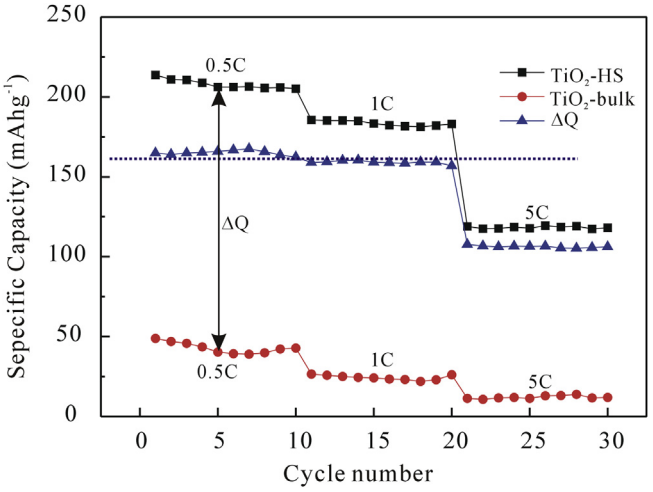

Fig. 7. Discharge capacity cycling performance of TiO_2-HS and TiO_2-bulk from 1.0 to 3.0 V at various rates.

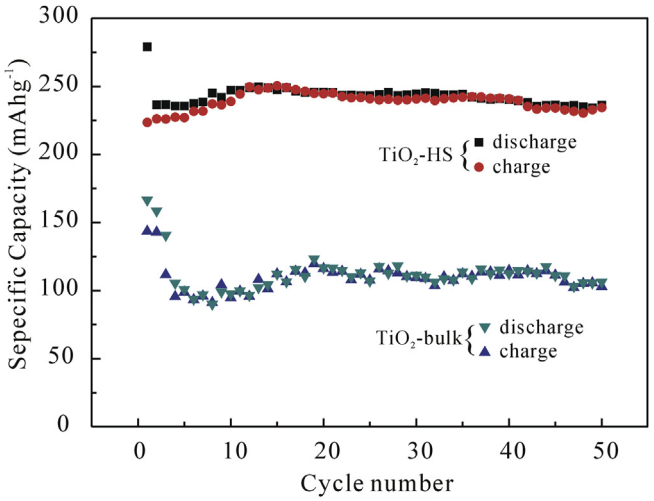

Fig. 8. Charge and discharge capacity cycling performance of TiO_2-HS and TiO_2-bulk from 1.0 to 3.0 V at 0.1 C.

dash line. It has been shown in Fig. 5 that the plateau capacities in discharge curves of TiO_2-bulk and TiO_2-HS are almost identical at 0.1 C. So the values of ΔQ approximately embody the contribution of additional surface capacity to the total capacity. This observation confirm the assumption we made previously that the capacity loss at 0.5 C and 1 C mainly come from the polarization of insertion of lithium into TiO_2 lattice, the polarization of additional surface capacity of TiO_2-HS is small enough to be ignored. However, at 5 C rate the value of ΔQ is dramatically smaller than the ones at 0.5 C and 1 C rates. This is reasonable because at this discharge rate the polarization of additional surface capacity is markedly increased and can not to be ignored.

Besides the rate performance of TiO_2-HS, the capacity retention is also investigated because capacities fading are always shown for TiO_2 hollow spheres [16–20]. Fig. 8 presents the data in terms of cycling performance of TiO_2-HS and TiO_2-bulk. The TiO_2-HS have better capacity retention than TiO_2-bulk and deliver a reversible lithium storage capacity of 230 $mAhg^{-1}$ after 50 cycles at 0.1 C. Coarse grained TiO_2-bulk show a fast capacity fading in the initial ten cycles and a stable capacity of about 100 $mAhg^{-1}$ in the following cycles. The stable cycle performance of TiO_2-HS is shown during the total 50 cycles due to its highly reversible surface capacities and accommodation of phase transformation within nanostructure.

4. Conclusions

Uniform and monodispersed TiO_2 hollow spheres with nanoporous titania shell were prepared by using carboxyl-functionalized polystyrene spheres as templates. Studies show that the TiO_2 hollow spheres have higher discharge capacity and better capacity retention at 0.1, 0.5 C, 1 C and 5 C rates than those of bulk TiO_2 with coarse grain. The better electrochemical performance of TiO_2 hollow spheres is attributed to the additional capacity of surface lithium insertion and extraction. Due to the facility and reversibility of lithium storage in surface and the sluggish and irreversibility of lithium ion diffusion in TiO_2 lattice, higher discharge capacity and better capacity retention are observed for TiO_2 hollow spheres. We expect that these TiO_2 hollow spheres will provide new possibilities for electrode materials of advance lithium ion batteries with high power densities. The mechanism of the formation of additional surface capacity for anatase TiO_2 hollow should be studied further.

Acknowledgments

This work was supported by the National Natural Science Foundation of China (No. 20803056) and the Fundamental Research Funds for the Central Universities (No. 2012-Ia-039; No. 2010-Ia-013).

References

[1] B. Scrosati, J. Garche, Journal of Power Sources 195 (2010) 2419–2430.
[2] Z. Yang, D. Choi, S. Kerisit, K.M. Rosso, D. Wang, J. Zhang, G. Graff, J. Liu, Journal of Power Sources 192 (2009) 588–598.
[3] D. Deng, M.G. Kim, J.Y. Lee, J. Cho, Energy & Environmental Science 2 (2009) 818–837.
[4] X. Su, Q.L. Wu, X. Zhan, J. Wu, S.Y. Wei, Z.H. Guo, Journal of Materials Science 47 (2012) 2519–2534.
[5] V.G. Pol, S.-H. Kang, J.M. Calderon-Moreno, C.S. Johnson, M.M. Thackeray, Journal of Power Sources 195 (2010) 5039–5043.
[6] M. Wagemaker, G.J. Kearley, A.A. van Well, H. Mutka, F.M. Mulder, Journal of the American Chemical Society 125 (2003) 840–848.
[7] F. Gligor, S.W. de Leeuw, Solid State Ionics 177 (2006) 2741–2746.
[8] S. Yoon, B.H. Ka, C. Lee, M. Park, S.M. Oh, Electrochemical and Solid State Letters 12 (2009) A28–A32.
[9] L. Kavan, J. Rathousky, M. Gratzel, V. Shklover, A. Zukal, Journal of Physical Chemistry B 104 (2000) 12012–12020.
[10] H. Qiao, L. Xiao, L. Zhang, Electrochemistry Communications 10 (2008) 616–620.
[11] H.B. Wu, J.S. Chen, H.H. Hng, X.W. LOu, Nanoscale 4 (2012) 2526–2542.
[12] M.L. Sushko, K.M. Rosso, J. Liu, Journal of Physical Chemistry Letters 1 (2010) 1967–1972.
[13] J. Wang, J. Polleux, J. Lim, B. Dunn, Journal of Physical Chemistry C 111 (2007) 14925–14931.
[14] T. Okumura, T. Fukutsuka, A. Yanagihara, Y. Orikasa, H. Arai, Z. Ogumi, Y. Uchimoto, Chemistry of Materials 23 (2011) 3636–3644.
[15] C.H. Jiang, M.D. Wei, Z.M. Qi, T. Kudo, I. Honma, H.S. Zhou, Journal of Power Sources 166 (2007) 239–243.
[16] B. Song, S. Liu, J. Jian, M. Lei, X. Wang, H. Li, J. Yu, X. Chen, Journal of Power Sources 180 (2008) 869–874.
[17] X.W. Lou, L.A. Archer, Advanced Materials 20 (2008) 1853–1858.
[18] J.P. Wang, Y. Bai, M.Y. Wu, J. Yin, W.F. Zhang, Journal of Power Sources 191 (2009) 614–618.
[19] J.S. Chen, D.Y. Luan, C.M. Li, F.Y.C. Boey, S.Z. Qiao, X.W. Lou, Chemical Communications 46 (2010) 8252–8254.
[20] Y. Wang, X.W. Su, S. Lu, Journal of Materials Chemistry 22 (2012) 1969–1976.
[21] S.J. Ding, J.S. Chen, Z.Y. Wang, Y.L. Cheah, S. Madhavi, X.A. Hu, X.W. Lou, Journal of Materials Chemistry 21 (2011) 1677–1680.
[22] F. Zhang, Y. Zhang, S.Y. Song, H.J. Zhang, Journal of Power Sources 196 (2011) 8618–8624.
[23] M. Wagemaker, R. van de Krol, A.P.M. Kentgens, A.A. van Well, F.M. Mulder, Journal of the American Chemical Society 123 (2001) 11454–11461.
[24] G. Sudant, E. Baudrin, D. Larcher, J.M. Tarascon, Journal of Materials Chemistry 15 (2005) 1263–1269.
[25] H. Xiong, H. Yildirim, E.V. Shevchenko, V.B. Prakapenka, B. Koo, M.D. Slater, M. Balasubramanian, S. Sankaranarayanan, J.P. Greeley, S. Tepavcevic, N.M. Dimitrijevic, P. Podsiadlo, C.S. Johnson, T. Rajh, Journal of Physical Chemistry C 116 (2012) 3181–3187.
[26] S.H. Kang, J.B. Goodenough, L.K. Rabenberg, Electrochemical and Solid State Letters 4 (2001) A49–A51.
[27] R. van de Krol, A. Goossens, E.A. Meulenkamp, Journal of the Electrochemical Society 146 (1999) 3150–3154.
[28] M. Wagemaker, W.J.H. Borghols, E.R.H. van Eck, A.P.M. Kentgens, G.L. Kearley, F.M. Mulder, Chemistry-a European Journal 13 (2007) 2023–2028.